Lambert Wanninger*, Melanie Thiemig, and Volker Frevert

Multi-frequency quadrifilar helix antennas for cm-accurate GNSS positioning

https://doi.org/10.1515/jag-2021-0042
Received June 29, 2021; accepted August 18, 2021

Abstract: For a few years now, GNSS multi-frequency quadrifilar helix antennas (QHA) are available to be used for precise GNSS applications. We performed test measurements with two types of multi-frequency QHA and compared them with a geodetic patch antenna. Although code and carrier phase noise and high-frequent multipath was determined to be larger as compared to the geodetic antenna, the fast-static horizontal coordinate accuracies are on the same level and demonstrate cm-accuracy capability. One of the QHA types exhibited an increased susceptibility to near-field multipath effects which resulted in a degraded accuracy of the vertical coordinate component.

Keywords: GNSS, quadrifilar helix antennas, cm-accurate positioning

1 Introduction

Quadrifilar helix antennas (QHA) consist of an array of four helically shaped resonant antenna elements wrapped around a cylinder [6, 4]. The antenna elements can be produced by printing to reduce costs. The antenna size can be controlled by using dielectric substrates for the antenna core.

The use of quadrifilar helix antennas (QHA) for GNSS receiving antennas was discussed as early as 1990 [9]. Whereas single-frequency QHA have been in wide use for handheld GNSS devices [4], only recently multi-frequency stand-alone antennas have been offered mainly for precise GNSS positioning of light-weight unmanned aerial vehicle (UAV). The QHA are especially suited for UAV because of their low weight as compared to high-quality patch antennas.

QHA produce a circularly polarized hemispherical radiation pattern with the rotation of the circular polarization being defined by the curling direction of the monofilars. It is important that the antenna's main lobe points to the sky in order to receive the GNSS signals with maximum antenna gain. On the other hand, QHA may suffer from backlobes that can make the antenna more susceptible to reception of multipath signals from below the antenna horizon. Increasing the length of a QHA can attenuate the undesired backward antenna lobes [6].

However, the cylindrical shape and longer length as compared to patch antennas makes the QHA unsuitable for certain rover applications [4], as e. g. its use on aircrafts. The applications we had in mind when testing two types of QHA were classical GNSS surveying work either as real-time (RTK) or in post-processing mode. In these applications the cylindrical shape and the antenna size causes no limitations whereas the low antenna weight can be of advantage. Another asset of the multi-frequency QHA that have become available in the past few years is their reasonable retail price.

After an introduction to the tested antennas and the further equipment (Section 2), we present results of the quality assessment of code and carrier phase observables obtained with QHA and a patch antenna (Sections 3.1). In a further test, we determined the susceptibility of the antenna types to near-field multipath (Section 3.2) and performed antenna phase center determinations (Section 3.3). Finally, extensive field tests were conducted in order to determine the performance of the antenna types in precise fast-static applications (Section 4).

Throughout the text, we name the signals in accordance with the RINEX 3 conventions [7] with one capital letter for the GNSS: G, R, E, C for GPS, GLONASS, Galileo, BeiDou, respectively, one digit for the frequency: 1 ... 8, and one capital letter for the tracking mode: e. g. C, I, P, R, W. Please, refer to [7] for more information on these abbreviations.

2 Equipment

In this study, we tested two types of QHA and analyzed their observations and positioning results. We had available 2 Maxtena M7HCT-A-SMA [12] and 4 Tallysman HC975 [13]. In addition, we used two GNSS patch antennas of type

***Corresponding author: Lambert Wanninger,** Geodätisches Institut, Technische Universität Dresden, Dresden, Germany, e-mail: lambert.wanninger@tu-dresden.de, ORCID: https://orcid.org/0000-0002-7448-5528
Melanie Thiemig, Volker Frevert, Geodätisches Institut, Technische Universität Dresden, Dresden, Germany, e-mails: melanie.thiemig@tu-dresden.de, volker.frevert@tu-dresden.de

Table 1: Technical data of the two kinds of QHA antennas and the geodetic antenna NavXperience NAX3G+C.

Antenna	Maxtena M7HCT-A-SMA	Tallysman HC975	NavXperience NAX3G+C
Frequencies	1192–1231 MHz	ca. 1164–1240 MHz	1150–1300 MHz
	1559–1606 MHz	ca. 1559–1610 MHz	1525–1610 MHz
Size (lower diameter × height)	3.4 cm × 5.1 cm	4.4 cm × 6.2 cm	12.7 cm × 7.2 cm
Weight	25 g	42 g	385 g
Connector	SMA, centered	SMA, centered	TNC, off-centered
Mount	–	3 screws (2.5 mm)	5/8″ thread

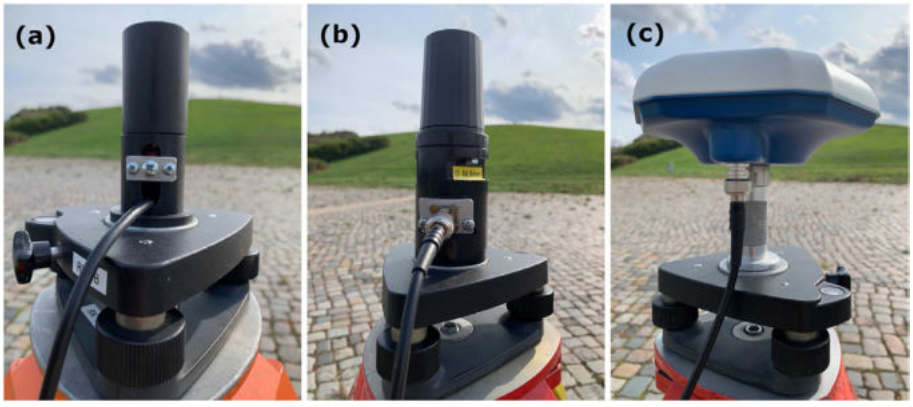

Figure 1: The three antenna types used in this study: (a) Maxtena M7HCT, (b) Tallysman HC975, (c) NavXperience 3G+C.

NavXperience NAX3G+C [5, 14] to either compare the observation properties with those of the two types of QHA (Sections 3.1, 3.2) or to determine reference coordinates of field stations (Section 4). In the further text we will refer to the two QHA types as M7HCT and HC975, and to the NavXperience NAX3G+C antenna as 3G+C.

Table 1 lists some of the technical specifications of the three antenna types as taken from the technical documentations of their manufacturers [12, 13, 14]. All three antennas are designed to receive a wide range of GNSS signal frequencies. However, the frequency ranges of these QHA do not include the following frequency bands:

- M7HCT: G5/E5/C5 (1176.45 MHz), R2 (ca. 1246 MHz), C6 (1268.52 MHz), and E6 (1278.75 MHz),
- HC975: R2 (ca. 1246 MHz), C6 (1268.52 MHz), and E6 (1278.75 MHz).

Nevertheless, the antennas received signals also on these frequencies and we processed these observations like all other observations. It can be expected that the antennas perform worse at these excluded frequencies as compared to those frequencies the antennas are designed for.

QHA and patch antennas differ considerably in their design and consequently in their size and weight. The QHA go without an internal or external ground plane and, thus, they are much smaller and their weight amounts to only about 10 % of a geodetic patch antenna.

The two types of QHA were not designed to be used on tribrach and tripod. The antenna cable connector is located at the center of the antenna bottom. This makes it difficult to quickly set-up the antenna on tribrach and tripod. Therefore, we designed and built adapters for the two types of QHA which serve as connectors to the tribrach and simplified the antenna set-up by guiding the antenna cable to one side. The adapters are made from polyoxymethylene.

Most geodetic antennas have markings indicating which part of the antenna should be aligned to true north. This alignment is of importance to correctly apply antenna phase center corrections to the observation data. If such a marker is missing, there is a convention to use the off-centered antenna cable attachment point as the north marker, e. g. [11]. The two types of QHA exhibit no such marker and even their cable connectors are centered and cannot be used as a substitute. Thus, we had to decide on an arbitrary direction to be used as horizontal reference direction for each individual QHA antenna.

All GNSS observations were performed using Septentrio PolaRx5 receivers, all with identical receiver settings. The near-field multipath test (Section 3.2) and the an-

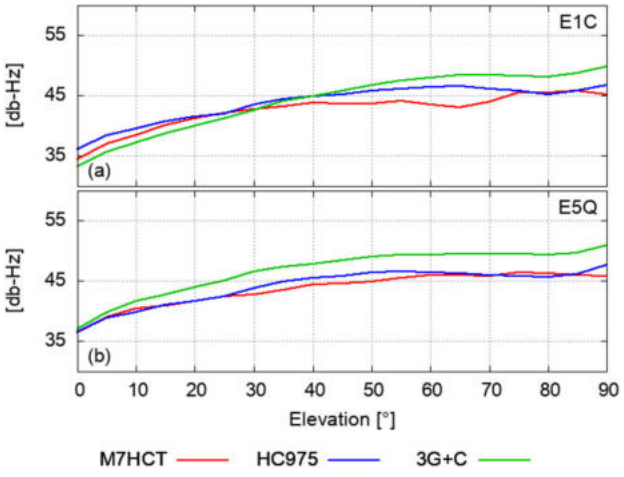

Figure 2: Elevation dependent C/N_0 of signals E1C and E5Q.

tenna calibration (Section 3.3) required a local GNSS reference station. We used a choke ring antenna of type Javad RingAnt-DM JVDM connected to a Septentrio PolaRx5. All GNSS data processing was performed using modules of the WaSoft software package.

3 First experiments and antenna calibration

3.1 Observation quality

For the first analysis steps, 24 h data sets of static observations were gathered with the two QHA and in addition with the patch antenna 3G+C. The antennas were set in a roof-top environment without signal obstructions and low multipath level. All three antennas occupied the same station for subsequent 24 h periods. The connected Septentrio PolaRx5 receiver was set to collect all available signals of GPS, GLONASS, Galileo and BeiDou.

The recorded C/N_0 values of all signals and antennas show the typical elevation-dependence known from geodetic type GNSS antennas with weaker signals at lower elevation angles and maximum signal levels above about 60 deg of elevation. The two types of QHA behave in a very similar way: the recorded C/N_0 values are often slightly smaller than those of the patch antenna, however at low elevation angles this difference gets smaller or the signal strength of the two QHA even exceeds those of the patch antenna (Fig. 2).

In order to compare the antenna properties for all available signals and frequencies we computed average C/N_0 values for each signal and an elevation range from 10 to 30 deg. Figure 3 shows the results for those 16 GNSS signals with sufficient transmitting satellites in space. Please note that some of the signals use identical frequencies but nevertheless differ in their modulation and the receiver tracking mode. Identical frequencies are used by the following groups of signals: G5Q/E5Q/C5P (1176.45 MHz), E7Q/C7I (1207.14 MHz), and G1C/E1C/C1P (1575.42 MHz).

In the lower frequency band from 1176.45 MHz (G5Q/E5Q/C5P) to 1278.75 MHz (E6C) the QHA signal strength values are smaller than those of the 3G+C. In the higher frequency band, they are usually slightly larger. Largest differences in signal strength are found for some of those QHA signals with frequencies for which these antennas were not designed: R2C, C6I, E6C. The M7HCT also exhibits weak signal strength for R1C (ca. 1602 MHz).

Using the same data sets, we determined code noise and multipath levels for all 16 signals. We used the MP (multipath) linear combination of code observations and dual-frequency carrier phase observations, which is some-

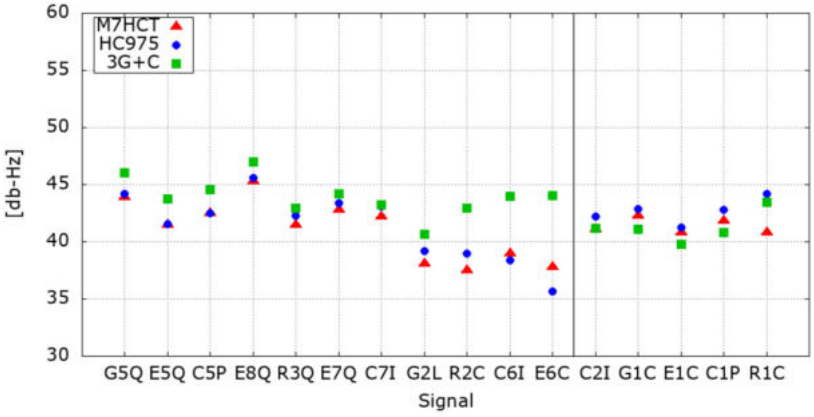

Figure 3: Average C/N_0 values in order of the signals' frequencies for elevation range 10 to 30 deg.

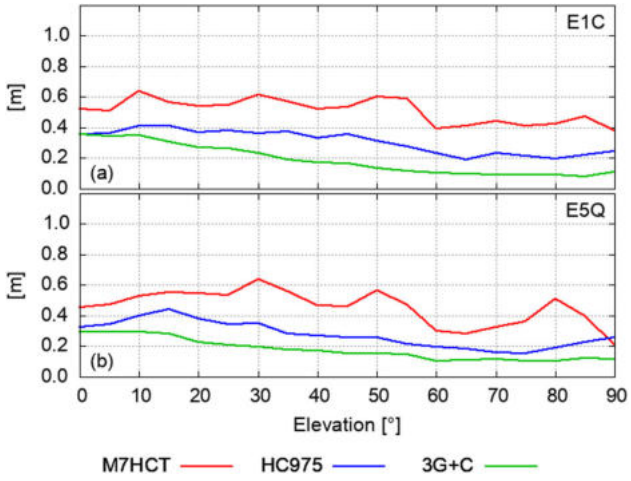

Figure 4: Elevation dependent RMS(MP) of signals E1C and E5Q.

times also called CMC (code minus carrier) linear combination [1, 3]. Time series of this multipath combination are dominated by code noise and code multipath. We extract this information by computing elevation dependent RMS values as shown in Figs. 4 and 5.

Here, the differences among the 3 tested antennas are much larger as compared to the signal strength values. The QHA always show a higher level of code noise/multipath as compared to the patch antenna. Furthermore, the MP values are always larger for the M7HCT as compared to the HC975. Whereas, the patch antenna shows a clear elevation-dependence of its MP-values with smaller values for larger elevation angles, this elevation-dependence is not so pronounced for the two QHA (Fig. 4).

The RMS(MP) values in the elevation range of 10 to 30 deg (Fig. 5) exhibit a clear ranking order of the three antenna types: the patch antenna 3G+C shows a code noise/multipath level of 0.4 m on average of all signals, the corresponding HC975 level is higher on average by approximately 30 % and the M7HCT level is higher on average by ca. 70 %. In the higher frequency band, the differences between 3G+C and HC975 are much smaller as compared to the lower frequency band.

In order to determine carrier phase noise and high-frequent multipath levels for all three antennas we observed short baselines with pairs of the same antenna type in static mode. Here again, the antennas were set in a rooftop environment without signal obstructions and low multipath level. All three pairs of antennas occupied the same stations for subsequent 24 h periods.

In the short baselines between the pairs of antennas, the carrier phase ambiguities were fixed to integer values and afterwards single-difference residuals were analyzed with respect to their elevation-dependent noise/multipath level. In this and all further analysis of the carrier phase observations, we combined signals with identical frequencies and, thus, present the results as a function of signal frequency.

The elevation-dependent carrier-phase noise and high-frequent multipath is shown in Fig. 6 for two selected frequencies: 1575.42 MHz (G1/E1/C1) and 1176.45 MHz (G5/E5/C5). In both cases, the QHA measurements show a higher noise level as those with the patch antenna. The M7HCT exhibits the largest high-frequent errors. The carrier-phase observations of all three antennas demonstrate a clear elevation dependence.

Again, we looked at all signal frequencies in the elevation range 10 to 30 deg. The RMS values show a clear ranking order of the three antenna types: the patch antenna 3G+C shows a carrier-phase noise and high-frequent multipath level of 4.6 mm on average of all frequencies, the corresponding HC975 level is higher on average by almost 40 % and the M7HCT level is higher on average by

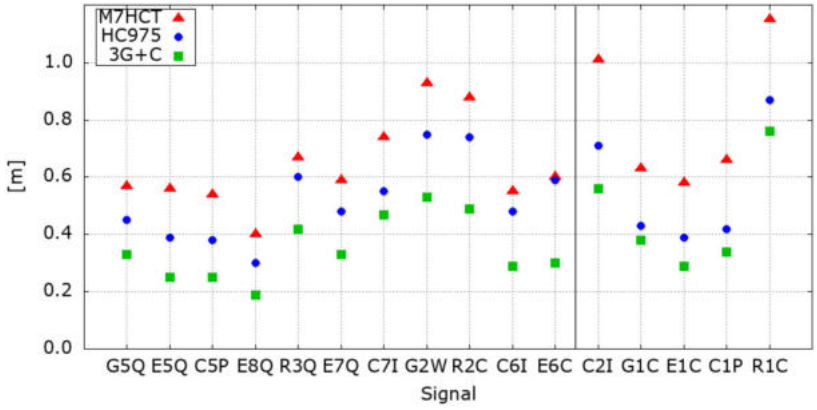

Figure 5: RMS(MP) values in order of the signals' frequencies for elevation range 10 to 30 deg.

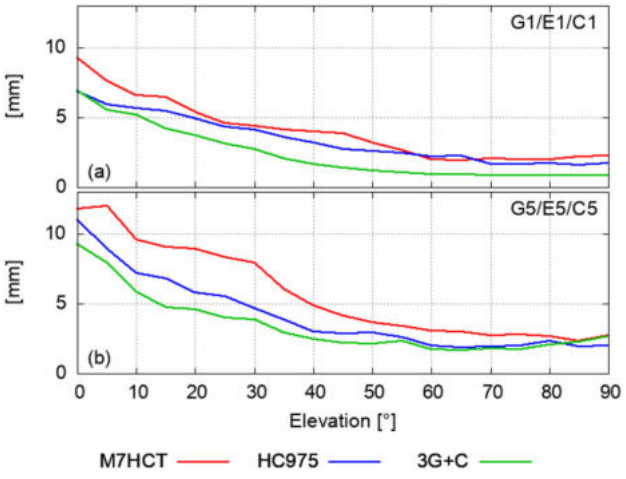

Figure 6: Elevation dependent carrier phase noise and multipath in a short baselines of identical antenna types for signals G1/E1/C1 (1575.42 MHz) and G5/E5/C5 (1176.45 MHz).

almost 70 %. In the lower frequency band, the differences are larger. In the higher frequency band, the RMS values of the QHA are larger by approximately 30 % as compared to the patch antenna.

3.2 Near-field multipath test

The effect of multipath on carrier-phase observations as determined in the last section relates to high-frequent multipath effects only. They are caused by distant (1 m and more) reflectors which cause high-frequent multipath effects with periods of a few to many minutes for GNSS satellites in MEO (medium earth orbit) heights. If the reflectors are closer to the antenna, multipath gets long-periodic and can hardly be separated from the estimated coordinates, i. e. multipath effects act as a bias to the coordinates. This near-field multipath may vary considerably as a function of antenna height, i. e. changes in the antenna height produce changes in the near-field multipath and, thus, in the multipath biases which affect the estimated coordinates, see e. g. [2, 10].

In order to determine the size of this near-field multipath for each of the antenna types, we performed the following experiment. In the roof-top environment with low multipath-level we determined short baselines between the reference antenna and each test antenna twice. The first observation period of several hours was performed with the test antenna in a low position and the second observation period of again several hours was performed with the test antenna in a high position. The height difference between low and high position, which was realized by a connecting bar, amounted to exactly 1.2658 m (Figs. 8 and 9). This height difference was determined from the difference of the two GNSS baseline results. The comparison of determined and known height difference provides information of the antennas' susceptibility to multipath.

Near-field multipath effects change between low and high antenna position as a function of the selected height difference and the signal wavelengths. A single such experiment with single-frequency GNSS observation may accidentally yield a perfect height difference determination. Therefore, such experiments must either be repeated with several height differences or several signals with different wavelengths must be evaluated. We followed the second approach and determined the height differences simultaneously on the 10 presently available GNSS frequencies with wavelengths between 18.7 and 25.5 cm.

We expect that the determined height differences agree very well with the known height difference for anten-

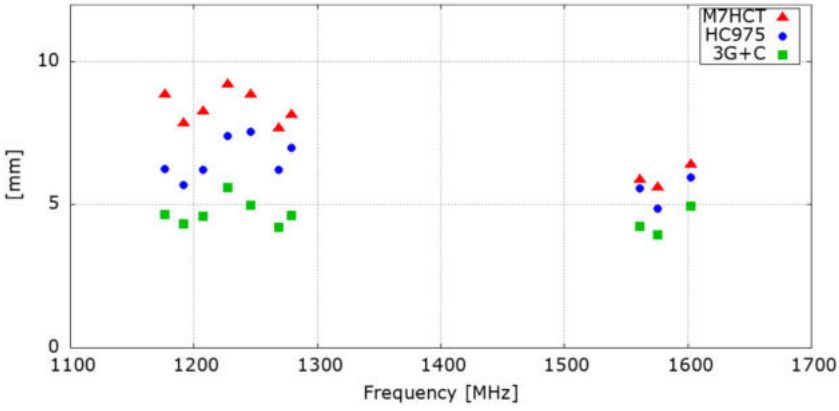

Figure 7: Carrier phase noise and multipath (RMS values) in a short baselines of identical antenna types for elevation range 10 to 30 deg of those frequencies and signals with sufficient broadcasting satellites in space.

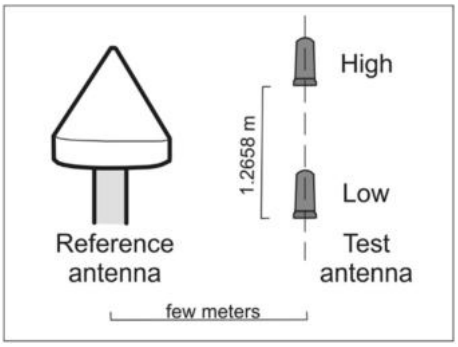

Figure 8: Set-up of the high-low near-field multipath test.

Figure 9: Quadrifilar helix antennas in low and high position.

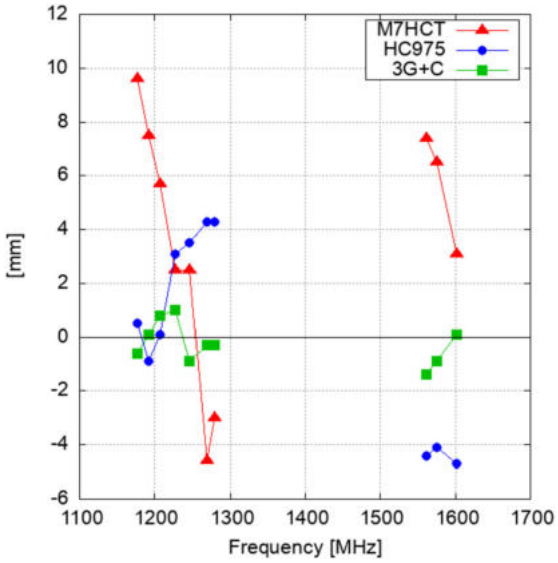

Figure 10: Height difference errors of low set-up minus high set-up in the short baseline to the reference station as a function of frequency.

Figure 11: One of the QHA on the calibration device DRB2.

nas which show little susceptibility to multipath. On the other hand, antennas which are highly susceptible to near-field multipath will show larger variations of the height difference errors.

The three different test antennas show very different results (Fig. 10). Whereas the height difference errors of the patch antenna 3G+C do not exceed 1.5 mm, much larger height errors were determined for the two QHA. The height difference errors of HC975 vary between –5 and +5 mm and the ones of M7HCT even reach 10 mm in maximum. The conclusion is that the three antenna types are susceptible to near-field multipath on very different levels: the 3G+C is least affected, HC975 experiences larger multipath effects, and the effects on M7HCT are the largest.

3.3 Antenna calibration

Phase-center offsets (PCO) and variations (PCV) were determined for all six individual QHA by field calibration. We used the DRB2 rotational device (Fig. 11), which enables observations in four azimuthal orientations per minute but does not perform an antenna tilting [8]. The observations in various azimuthal orientations enable the determination of phase center variations for the complete upper hemisphere and they also help to mitigate carrier-phase multipath effects on the horizontal PCO components. However, the height components are still affected by local multipath. The local reference station equipped with a JavRingAnt_DM JVDM antenna served as reference. Since the baseline between the reference antenna and the QHA amounts to just a few meters, all atmospheric influences are eliminated and do not degrade the calibration results. Each calibration session lasted at least 24 h.

The calibration results consist of PCO and PCV. Figures 12 and 13 depict PCO results for all available GNSS-frequencies. PCO values of adjacent frequencies are con-

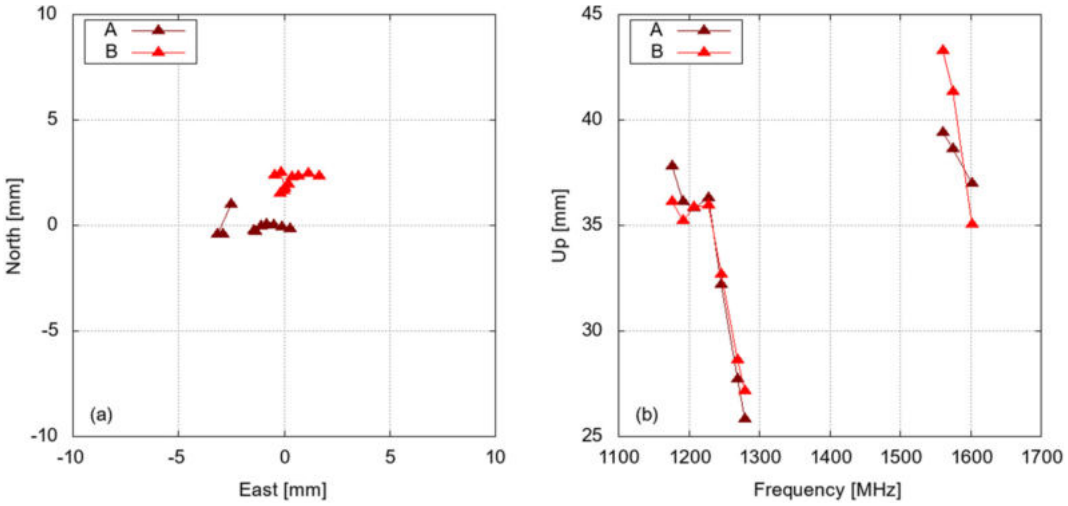

Figure 12: Calibration results of 2 individual M7HCT antennas on 10 frequencies: phase center offsets horizontally and the up-component as a function of frequency.

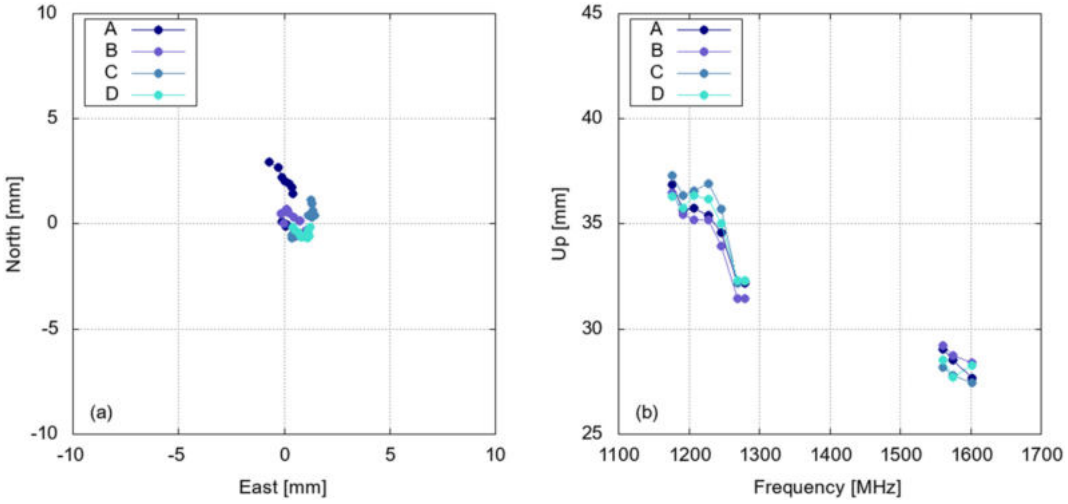

Figure 13: Calibration results of 4 individual HC975 on 10 frequencies: phase center offsets horizontally and the up-component as a function of frequency.

nected by lines. Figure 15 shows average PCV pattern of two selected frequencies for each type of QHA.

Since the QHA housings are rotational symmetric and there is no marker to define a reference direction, we added an arbitrary marker to each individual antenna to be aligned to true north. Therefore, the horizontal PCO as shown in Figs. 12a, 13a could be twisted. The results, however, show that all horizontal PCO are smaller a few millimeters and since the PCV pattern did not reveal any significant azimuthal variations, it can be concluded, that the azimuthal orientation of the individual antennas is not of importance as long as horizontal accuracies of some millimeters are sufficient.

Also, the vertical PCO (Figs. 12b, 13b) of the individual antennas exhibit good agreement among those of the same QHA type. The M7HCT show a clear frequency dependence of their vertical PCO (Fig. 12b) but we cannot rule out that these variations in the order of 1 cm are caused by near-field multipath effects (cf. Section 3.2). The manufacturer of M7HCT published vertical PCO values of 36.2 mm for the higher frequency band and of 34.8 mm for the lower frequency band [12]. These values could be confirmed but remaining height errors of several millimeters, whether they are caused by the phase center uncertainty or near-field multipath, should be expected in practical applications.

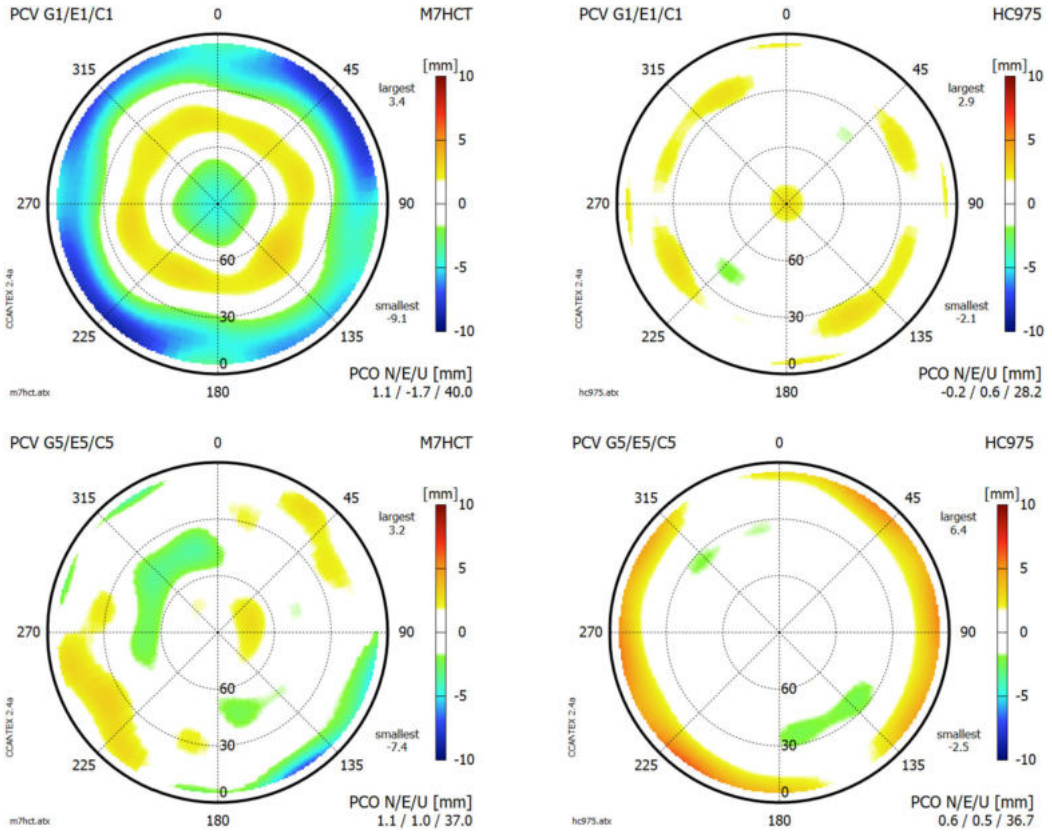

Figure 14: Mean calibration results of 2 M7HCT antennas (left) and of 4 HC975 antennas (right) on frequencies G1/E1/C1 and G5/E5/C5.

The frequency-dependence of the vertical PCO of HC975 seems to be smaller (Fig. 13b). In the lower frequency band and, with the exception of E6/C6 frequencies, the average vertical PCO amounts to 36 mm with individual deviations of a few millimeters in maximum. In the higher frequency band, the average vertical PCO amounts to 28 mm. The manufacturer of HC975 published vertical PCO values of 38 mm for the lower frequency band and of 32 mm for the higher frequency band [13]. Thus, our calibration results yielded slightly smaller values. In addition, our results for the vertical PCO values for E6/C6 are significantly different (32 mm). But please remember that the manufacturer does not recommend the use of this antenna type in the frequency range of E6/C6.

The determined PCV reach up to about 1 centimeter for M7HCT, whereas they do not exceed a few millimeters for HC975. The agreement among the PCV of the individual antennas was so good, that we could combine them to PCV of the antenna types (Fig. 14).

The antenna calibrations revealed a good agreement of the phase centers of the individual antennas of each type. Horizontal PCO are fairly small and need no correction for cm-accurate positioning. Vertical PCO are dependent on the signal's frequency and must be corrected to be able to obtain cm-accuracy. PCV of the HC975 are so small that a correction seems not to be necessary. However, the elevation-dependence of the M7HCT PCV requires corrections.

4 Field measurements and achievable accuracies

Field measurements were performed on 15 stations with all three antenna types. Each station was occupied by each of the three antenna types for a period of 2 hours. The stations were selected to include favorable GNSS sites with very little obstructions and also adverse GNSS sites with signals obstructions by vegetation and buildings but still suitable for cm-accurate GNSS positioning (Fig. 15). All observations were performed with the antennas on stable tripods (cf. Fig. 1). The Septentrio PolaRx5 receivers collected observations of all 4 GNSS: GPS, GLONASS, Galileo, and BeiDou.

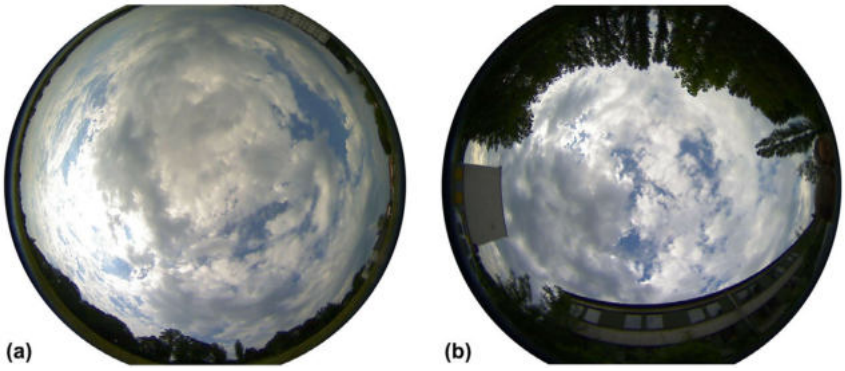

Figure 15: Examples of rover station surroundings of (a) a favorable station and of (b) an adverse station. The photos were recorded using a fisheye objective.

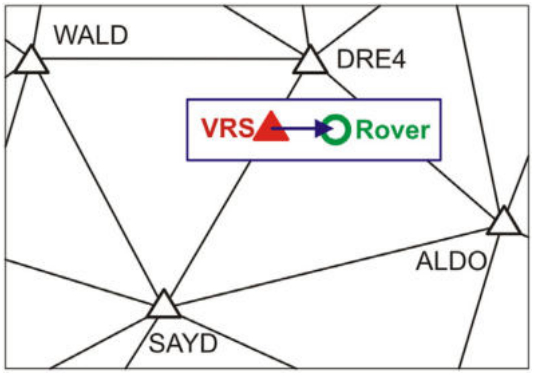

Figure 16: Continuously operating GNSS stations of the German SAPOS network surrounding the field measurement sites and used for VRS computation and consequently for baseline results.

The positioning results were determined in post-processing mode. We used virtual reference stations (VRS) as the reference for relative positioning based on ambiguity-fixed carrier phase observations. The VRS were computed from the surrounding continuously operating reference station of the German SAPOS network (Fig. 16). All rover sites are located in the southern part of the area of the city of Dresden, at distances between 3 and 6 km from the continuously operating reference station DRE4, and either within the triangle WALD-DRE4-SAYD or within SAYD-DRE4-ALDO.

The VRS provide multi-frequency observations of all 4 GNSS. At the favorable sites 28.5 satellites were available on average and above an elevation mask angle of 10 degrees. At the adverse sites this number is smaller and reaches 24.8 satellites. No significant differences among the three antennas could be observed with respect to the number of observed GNSS signals. The baseline results VRS – rover are based on dual-frequency data processing of all 4 GNSS. We applied antenna phase center corrections to all observations. The QHA observations were corrected using the antenna type specific results which are partly shown in Fig. 14.

The results of the 2 h observation sessions of the 3G+C antennas were used as reference coordinates of all further evaluations. Each 2 h session was subdivided into 24 short sessions of 5 minutes each. Each 5 minutes session was processed independently and its results compared with the reference coordinates. Thus, for each antenna type there are 360 samples of 5 minutes sessions. 216 samples were collected at sites ranked as favorable and another 144 samples at sites ranked as adverse. We had to remove 0.6 %, 0.3 % and 0.6 % of all solutions as outliers for M7HCT, HC975 and 3G+C, respectively. All of them were caused by incomplete ambiguity fixing at one of the adverse stations. Thus, the success rate of ambiguity fixing was almost identical among all three antenna types. The higher noise and multipath level of the QHA code and carrier phase observations (cf. Section 3.1) seems not to cause any adverse effects on ambiguity fixing in fast-static mode.

The distribution of the coordinate errors of the 5 minutes sessions reveals fairly small differences among the three antenna types in the horizontal components (Fig. 17). A vast majority of all solutions displays horizontal coordinate errors of less then 1 cm. No biases can be observed.

In the vertical component, the ranges between minimum and maximum coordinate errors are very similar for all three antenna types. However, there are biases, especially a large bias of the M7HCT results with a median of −2.0 cm. HC975 vertical coordinate errors show a smaller bias of 0.7 cm. The vertical results of 3G+C show no bias. This, however, is no surprise since the reference coordinates had been determined from the same 3G+C data sets.

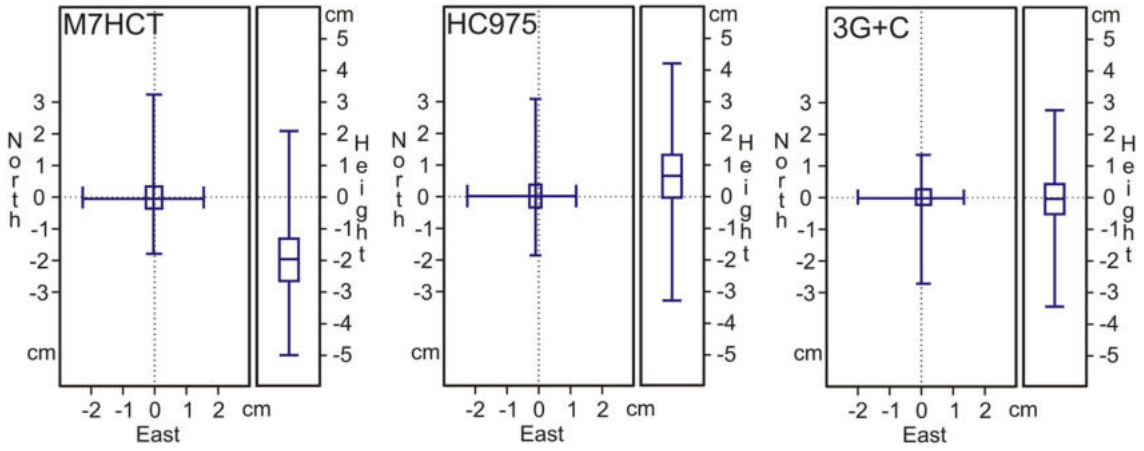

Figure 17: Distribution of coordinate errors of 5 minutes sessions (n = 360) as 2D (north/east) and 1D (height) box and whisker plots depicting percentile values for 0 (minimum), 25, 50 (median), 75, and 100 (maximum).

Table 2: RMS values of the coordinate errors of 5 minutes sessions in cm.

Antenna	9 favorable stations (n = 216) North/East/Height	6 adverse stations (n = 144) North/East/Height
M7HCT	0.73/0.42/2.08	0.70/0.42/2.50
HC975	0.49/0.41/1.02	0.70/0.33/1.51
3G+C	0.48/0.39/0.80	0.46/0.32/0.93

We suspect that this large vertical bias of the M7HCT results is caused by near-field multipaths effects. The high susceptibility of this antenna type to near-field multipath had already been shown in Section 3.2 of this paper. Near-field multipath effects differ between our antenna calibration on DRB2 (Section 3.3) and the field measurements on tripod and tribrach. With antennas not that susceptible to near-field multipath, this change of the antenna near-field environment does not cause significant vertical biases. However, in case of M7HCT the resulting bias exceeds a 1 cm threshold.

In a further step, we compared the 5 minutes session results of the favorable stations with those of the adverse stations. The RMS values as shown in Table 2 reveal slightly larger values for the adverse stations in the vertical components of all three antenna types. But in general, we were surprised to see that the overall performance does not differ very much between favorable and adverse stations. We attribute this result to the large number of available satellite signals.

The RMS values of Table 2 demonstrate again that all three antenna types produced results of similar quality for the horizontal components. The performance in the vertical components shows significant differences mainly due to the vertical bias for antenna M7HCT as discussed above.

5 Conclusions

Although the two tested multi-frequency QHA antennas perform slightly worse as compared to the geodetic patch antenna with respect to code and carrier phase noise and high-frequent multipath, the fast-static horizontal positing results are all on the same quality level. Centimeter accurate horizontal positioning results can easily be achieved with all three kinds of antenna types.

However, the results differ significantly in the vertical component, especially for one type of the QHA which exhibited a strong susceptibility to near-field multipath effects. They can cause systematic vertical coordinate errors in the order of one to a few centimeters. The other QHA type was less susceptible to near-field multipath and produced better results in the vertical component.

Considering the demonstrated performance of the QHA and their advantages with respect to weight and retail price, they should be considered as an alternative to geodetic patch antennas for a large number of applications.

References

[1] Braasch MS. Multipath. In *Springer Handbook of Global Navigation Satellite Systems*, Teunissen PJG, Montenbruck O (eds.). Springer International Publishing, Cham, 2017, 443-468. doi 10.1007/978-3-319-42928-1_15.

[2] Elósegui P, Davis JL, Jaldehag RTK, Johansson JM, Niell AE, Shapiro II. Geodesy using the Global Positioning System: The effects of signal scattering on estimates of site position. *J. Geophys. Res. Solid Earth* 100, B6 (June 1995), 9921–9934. doi 10.1029/95JB00868.

[3] Hauschild A. Combinations of Observations. In *Springer Handbook of Global Navigation Satellite Systems*, Teunissen PJG, Montenbruck O (eds.). Springer International Publishing, Cham, 2017, 583–604. doi 10.1007/978-3-319-42928-1_20.

[4] Maqsood M, Gao S, Montenbruck O. Antennas. In *Springer Handbook of Global Navigation Satellite Systems*, Teunissen PJG, Montenbruck O (eds.). Springer International Publishing, Cham, 2017, 505–534. doi 10.1007/978-3-319-42928-1_17.

[5] Popugaev AE, Wansch R. Multi-Band GNSS Antenna. In *Microelectronic Systems*, Heuberger A, Elst G, Hanke R (eds.). Springer Berlin Heidelberg, Berlin, Heidelberg, 2011, 69–75. doi 10.1007/978-3-642-23071-4_8.

[6] Rama Rao B, Kunysz W, Fante RL, McDonald KF. *GPS/GNSS antennas*. Artech House, Boston, 2013.

[7] Romero I. RINEX – The Receiver Independent Exchange Format Version 3.05 (IGS/RTCM RINEX Working Group), 2020. Retrieved from https://files.igs.org/pub/data/format/rinex305.pdf.

[8] Schmolke A, Wanninger L, Frevert V. Erste GNSS-Antennenkalibrierungen im Feldverfahren auf neuen Signalfrequenzen. *Zfv – Z. für Geodäsie Geoinformation Landmanagement* 5 (2015), 283–289. doi 10.12902/zfv-0083-2015.

[9] Tranquilla JM, Best SR. A study of the quadrifilar helix antenna for Global Positioning System (GPS) applications. *IEEE Trans. Antennas Propag.* 38, 10 (Oct 1990), 1545–1550. doi 10.1109/8.59766.

[10] Wanninger L. Correction of apparent position shifts caused by GNSS antenna changes. *GPS Solut.* 13, 2 (March 2009), 133–139. doi 10.1007/s10291-008-0106-z.

[11] NGS. Guidelines for New and Existing Continuously Operating Reference Stations (CORS), National Geodetic Survey, Silver Spring, MD, 2018. Retrieved from https://www.ngs.noaa.gov/PUBS_LIB/CORS_guidelines.pdf.

[12] Maxtena M7HCT-A-SMA. Retrieved from https://maxtena.com/products/gps/m7hct-a-sma-multi-frequency-active-antenna/.

[13] Tallysman HC975. Retrieved from https://www.tallysman.com/product/hc975-triple-band-helical-antenna-l-band/.

[14] NAX3G+C. Retrieved from https://navxperience.com/.